PCCP

Accepted Manuscript




ROYAL SOCIETY OF CHEMISTRY

www.rsc.org/pccp

Physical Chemistry Chemical Physics

ARTICLE

# Why is the electroanalytical performance of carbon paste electrodes involving ionic liquid binder higher than paraffinic binders? a simulation investigation

Received 00th January 20xx,
Accepted 00th January 20xx

DOI: 10.1039/x0xx00000x

www.rsc.org/

M. H. Ghatee,[a†] S. Namvar[a], A. R. Zolghadr[a], and F. Moosavi[b]

Recently, carbon paste electrodes (CPE) fabricated by using ionic liquid (IL) binder have shown enhanced electroanalytical performance over conventional paraffinic binder. Molecular dynamic (MD) simulations of graphite mixed with ionic liquid and with paraffine binder can unravel the potential atomistic factors responsible for such enhancement. Based on experimentally optimized binder/graphite mass ratio, reported crucial for such a performance, comprehensive simulations (at 323K) are performed by the ensembles involving ionic liquid binder (1-butyl-3-methylimidazolium hexafluorophsphate, $[C_4mim]PF_6$) and paraffine binder ($n$-$C_{20}H_{42}$) mixed with graphite comprising a large-size hexagonal-shaped double graphene plates. Structural analysis indicates either binder forms only a monolayer on graphite surface, covering the surface locally by IL but all-encompassing by paraffine. With charged and uncharged graphite, IL monolayer tends covering mainly the graphite center without approaching to edge planes. Contrary, monolayer of paraffine binder features covering uniformly center, near center, and the edge planes. Cations and anions of the IL form well-defined two dimensional pentagonal matrixes with characteristic high adsorption energy, almost 2.4 times higher than paraffine adsorption. Cation and anion coordination ability of IL is responsible for such a local distribution. The simulation of phenomena under experimental condition unravels a *strong* two-dimensional coordination property inherent to ionic liquid when distributed over graphite surface. This direct MD simulation comparison of IL properties with an organic liquid counterpart, made for the first time, can be used to explain the high electroanalytical performance (electron transfer) of CPE involving IL binder over paraffine binder.

## Introduction

Room temperature ionic liquids (ILs) have received much attention in different fields of chemistry and electrochemical industry.[1-7] Apart from many green chemistry applications,[8-14] recent experimental studies have shown that ILs possess unique feature exhibiting enhanced electrochemical performance when used as binder for fabrication of carbon paste electrode.[15-17] Taking the advantages of experimental observations and information on the privilege of IL binders over the conventional paraffinic ones, we investigate this problematic phenomenon from atomistic and IL/graphite structural point of view by performing a comprehensive MD simulations.

Carbon paste electrodes (CPE) are widely used in electroanalytical investigations for properties of biomedical compounds because of their high chemical inertness, wide potential window, and low background current.[18-20] Several forms of graphite from graphite powder to the highly oriented pyrolytic graphite and carbon nanotubes are among the material used for fabrication of these electrodes.[21] The response of carbon paste electrode for sensing chemical species has been subjected to vast variety of electroanalytical investigations. The particular properties of multi-wall carbon nanotube modified electrodes towards oxidation of biochemical compounds has been shown to be due to edge plane sites, occurring along the tubes or their open ends. For such enhanced electrochemical analysis, it has been argued that utilized electrode should optimally involves a large proportion of edge plane site,[22] which was explored by utilizing edge plane pyrolytic graphite.

The replacement of non-conductive paraffinic liquid with conductive IL in fabrication of carbon paste electrode is rather new. Liu et al. have fabricated a novel carbon paste electrode containing hydrophobic imidazolium-based IL and found that it possesses excellent electrocatalytic activity.[14] A glassy carbon electrode modified by a gel of carbon nanotubes and IL 1-octyl-3-methylimidazolium hexafluorophosphate, $[C_8mim]PF_6$, has been found successful for assay of dopamine in human blood serum.[13] Roznicka et al. have studied the silicate carbon electrode, modified with t-butylferrocene in $[C_4mim]PF_6$ and $[C_{12}mim]Tf_2N$ ILs, by cyclic voltammetry. They found that the efficiency of the electrode process is much higher than that in organic polar binder.[12] In general, these fascinating electrochemical performances have been attributed to the increase in the electron transfer rate when an IL binder is employed. By fabrication of carbon paste ionic liquid electrode (CPILE), a combination of many good features over

[a] Department of Chemistry, Shiraz University, Shiraz, 71946, Iran
[b] Department of Chemistry, Ferdowsi University of Mashhad, Mashhad, 91779, Iran

† Author for correspondence, Email: ghatee@susc.ac.ir mhghatee2@gmail.com (M.H. Ghatee). Electronic Supplementary Information (ESI) available: [Force fields parameters; pair correlation functions; distances of closest approach; average orientation of the imidazolium ring plane.]. See DOI: 10.1039/x0xx00000x

variety of CPE, from carbon nanotubes to edge plane graphite electrodes, all convey in one electrode.[21] One of the very influential characteristics of the proposed electrode (shown specifically using pyridinum-based IL[21]) is the higher rate of electron transfer process, which is believed to be due to the microstructure of the electrode surface modified by using IL binder. These excess performances depend on the structural preferences of carbon allotropic form.

Edge plane pyrolytic graphite notably have been applied to increase the performance of the CPEs,[23] while the excess performance is an advantage of IL over paraffine binder used in common electrodes.[24,25] The SEM analysis of carbon-binder has revealed that a smooth paste is produced by using IL against the coarse paste obtained by paraffine binder.[21] These features of the newly developed electrodes have arisen the question of how IL/graphite fine structure is responsible for such remarkable performances. This issue commences a more detailed investigation by MD as a strong tool to understand the basic atomistic reason and IL/graphite structural relationship.

So far, MD simulation of IL/graphite in the favor of electrochemical performance has been conducted from the more general view of adsorbate-adsorbent characteristics. A tightly bounded layered adsorption has been identified on the graphite surface, as it is not disturbed by the presence of second or next layer in the bulk IL. Profiles of different surface layered film were found to be similar.[26] Other simulation investigation involves the structure of electrical double layer between $[C_4mim]PF_6$ IL near a basal plane of charged and uncharged graphite.[27] A bilayer of $[C_1mim]Cl$ IL confined between two parallel graphite walls has been simulated to study the freezing transition from a liquid monolayer to a solid one.[28,29] All these simulations endeavored studying the bulk of ILs adsorbed on graphite or graphene.

Formation of electrical double layer (EDL) and the differential capacitance (DC) are linked to any adsorption of liquid (charged or uncharged) near solid surface (charged or uncharged), and provide vital information on adsorbate-adsorbent features. Full atomistic simulation of $[C_1mim]Cl$ at the neutral graphite surface has revealed monolayer formation of $[C_1mim]^+$ cations, which attracts $Cl^-$ anions leading to the formation of several distinct solvation layers at the surface. As a result, a tightly bonded first layer and a diffused loosely bonded second layer of ionic liquid were identified.[30] EDL and DC structures of $[C_4mim]PF_6$ and $[C_4mim]BF_4$ electrolytes near graphite as well as (001) and (011) gold electrode surfaces were found to be nearly the same.[31] Molecular modeling of physical phenomena taking place in electric double-layer capacitors is important to microelectronic industry and a summary provided by Zhao.[32]

Several researchers have investigated the microscopic adsorption structures of imidazolium-based ILs on the surfaces of graphene plates by density functional theory (DFT).[33-35] The results for $[C_4mim]PF_6$ adsorption indicates that $PF_6^-$ anion is adsorbed and interacted with the solid surface while interacting with the imidazolium ring plane of the $[C_1mim]^+$ cation.

In regards to microcapacitor fabrication, the structure of EDL responsible for capacitive effect of ionic liquids on graphene and carbon nanotube has been studied extensively.[36] In particular the electrical charge enhancement at the edges of the non-passiveated graphene has been brought under question. The role of different edge type on the capacitance also has been studied.[37-45] To date, however, no theoretical simulation investigation has not been undertaken to unravel the electroanalytical enhancement by ILs binder versus conventional binder in fabrication of carbon paste electrode.

Therefore, our primary goal is to unravel factors responsible for the high performance of the CPILE over the common CPE. We present the results of simulation studies of the mixtures of $[C_4mim]PF_6$ + graphite and $n$-$C_{20}H_{42}$ + graphite, as the basic ingredient of the carbon paste electrodes, by atomistic classical molecular dynamics simulation. The structure and organization of each binder adsorbed over charged and uncharged graphite surface will be simulated. The gap in nature of two binders demands exploration of their details structural relation with respect to graphite substrate. Simulation model ensembles are based on exact binder/graphite mass ratio, which found and optimized experimentally in open literature. Such exact modeling forms a key point to the problem we seek. Comparison with simulation adsorption of bulk binder on graphite surface leads to a rewarding conclusion. The simulated binding energies account for the difference in their electrochemical performances. The inherent coordination property of IL when confined in two dimensions becomes a strong tool which leads to high performance carbon paste electrode.

**Simulation Details:** A graphene plate is constructed out of $sp^2$-hybridized carbon atoms arranged in a two dimensional hexagonal pattern with $D_{6h}$ symmetry. The graphite for the mixture consists of a double graphene plate (with un-passivated edges) each containing 600 carbon atoms ($C_{600}$) as shown in Figure 1. Compared to other geometrical shape, the plate in hexagonal shape, **1**) introduces as much edge planes as possible, **2**) benefits adequate (two-dimensional) radial symmetry suitable for calculation of pair correlation function as a strong tool for structural analysis, and **3**) involves the type of non-functionalized edge structure, which has been found energetically more adhering to the real graphite plate than with infinite carbon atoms.[46, 47] In simulations, the status of every atom of optimized double-$C_{600}$ plate is set rigid relative to its all-neighboring atoms, while the relative motion of the two plates is set unrestricted. The hexagonal is quite large with edge plane length of 24.34 Å, long diameter of 46.27 Å and total surface area of 1392.05 $Å^2$.

An initially optimized double-$C_{600}$ plates (3.35 Å apart) is used as graphite component in all simulation mixtures. The two plates are parallel with ABAB… relative conformation (Figure 1(**B,C**)). Because carbon atoms are considered rigid, intramolecular part of potential function is omitted and hence the interaction potential energy is

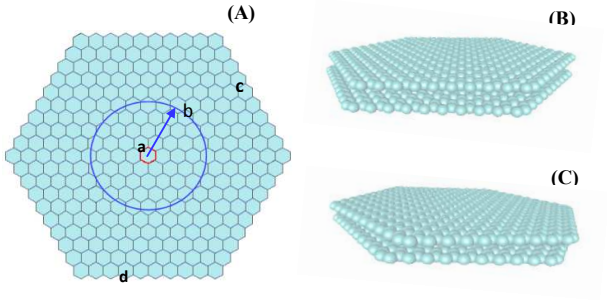


**Figure 1**. (**A**) Hexagonal $C_{600}$ graphene plate. Locations labeled: center (**a**, C_1), near center (**b**, C_106) and edge planes (**c**, C_512 and **d**, C_556). See text for (**B**) and (**C**).



 

$$V_{inter} = \sum_{i=1}^{599}\sum_{j>1}^{600}\left[V^{LJ}(r_{ij}) + V^{ES}(r_{ij})\right] \quad (1)$$

where $V^{LJ}$ is the LJ(12-6) and $V^{ES}$ is the electrostatic potential functions between atoms i and j located at $r_{ij}$. For carbon atom, the LJ potential parameter $\sigma_{ii}$ = 3.5 Å and $\varepsilon_{ii}$ = 0.276 kJ/mol.[48] For practical purpose, two cases are considered: **1**) each carbon atom having a neutral charge, **2**) each carbon atom having a (+1) and an electron with (-1) electrical charge unit. These cases will be referred to as *uncharged* and *charged* graphite, respectively. To construct the simulation ensembles, we follow the mass ratio (30/70, binder/graphite) found experimentally vital in fabrication of carbon past electrode at 323 K,[21,24] to achieve high electrochemical enhancement. Accordingly, ensemble of IL (or paraffine) consists of 22 $[C_4mim]PF_6$ (or 22 *n*-$C_{20}H_{42}$) per a double-$C_{600}$ plates.

With taking the simulation box large enough (81×81×81 Å$^3$) to prevent disturbing periodic neighboring boxes, two mixtures are prepared for each binder, by **1**) placing binder molecules equally over the outer surfaces of double-$C_{600}$, **2**) intercalating binder molecules in between the inner surfaces of the double-$C_{600}$. All simulations are carried out at 1 atm and 323 K, the thermal condition reported to be essential for electrode fabrication with the best electroanalytical performance.

Beginning with *NVE* ensemble ($r_{vdW}$ = 15.0 Å and $r_c$ = 30 Å), equation of motion is integrated by Verlet-leapfrog algorithm every 0.001 ps time step for 1 ns. The state of constant total energy is then attained after continuing the simulation for 4 more ns (0.002 ps time step) in *NVT* ensemble using Nose-Hoover thermostat.

Atomic charges for all simulations are obtained by full optimization of $[C_4mim]PF_6$ and *n*-$C_{20}H_{42}$ using DFT at B3LYP/6-311G level in GAUSSIAN 03 environment,[49] (Tables S1 and S2, Supplementary information), (labels, Figure 2). Eq. (1) is used to describe IL–graphite and *n*-$C_{20}H_{42}$–graphite interactions. Explicit fully flexible all-atom force field by Canongia Lopes *et al*. is used.[50] Parameters for modeling intra- and inter-molecular interactions of *n*-$C_{20}H_{42}$ is obtained from all-atom OPLS force field of Jorgensen et al.[51]

The total interaction potential energy has the form

$$V_{tot} = \sum_{bond\ i} 0.5k_{bi}(r_i - r_{eq})^2 + \sum_{angle\ i} 0.5k_{\theta i}(\theta_i - \theta_{eq})^2 + \quad (2)$$

$$\sum_{dihedral}\sum_{i=1}^{3} 0.5V_i\left[1 + (-1)^{i-1}\cos(i\Phi)\right] + \sum_{i=1}^{N-1}\sum_{j>1}^{N}\left\{4\varepsilon_{ij}\left[(\sigma_{ij}/r_{ij})^{12} - (\sigma_{ij}/r_{ij})^{6}\right]\right\} + \left(q_i q_j/4\pi\varepsilon_\circ r_{ij}\right) \quad (3)$$

where all terms have their usual meaning, and the cross term parameters $\varepsilon_{ij}$ and $\sigma_{ij}$ are given by combining and mixing rules.[52]

MD simulation provides an accurate practical means for analysis of structure by the pair correlation function, $g(r)$, using the trajectory histogram. It is formally defined as

$$g_{ij}(r) = (1/4\pi\rho_i r^2)(\Delta N_{ij}(r)/\Delta r) \quad (4)$$

with $\rho$ being number density; $\Delta N_{ij}$ is the number of atoms j within the shell of thickness $\Delta r$ located at distance $r$ from atom i. Atom-atom pair correlation functions provide a good estimate of spreading profile as well as structural relation between each binder monolayer molecules, in two dimensions, and graphite surface. All the simulations are performed by DL_POLY_2.17 software,[53] in parallel mode.

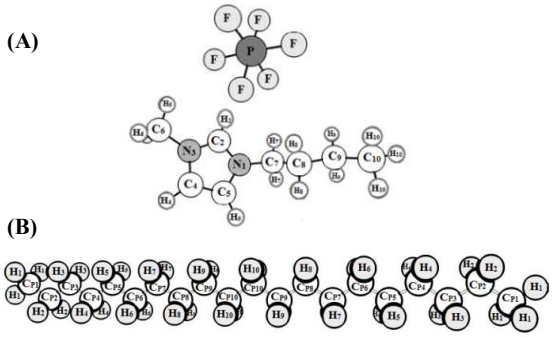


**Figure 2.** Structures and labeling: (**A**) $[C_4mim]PF_6$ , (**B**) *n*-$C_{20}H_{42}$.

## Results and discussion

The electrode accomplishment is significantly influenced by its compartment and molecular structure of the electrode/electrolyte interface through which electron transfer is occurred.[54-56] This structural relation, which is also widely of interest in multidisciplinary applications, is the main concern of present work. This issue can be covered by the correlation function, and its accuracy depends on sample size and the trajectory data sampled.

Surface area and edge planes of $C_{600}$ plate are chosen large enough for accurate adsorption simulation of the IL or paraffine. As simulation continues, the double-$C_{600}$ charged graphite plates (initially paralleled) are remained parallel but move about and freeze up to an ABAB… configuration (Figure 1(**B**)). With the uncharged graphite plates, ABAB… configuration is accompanied by relative distortion of the two plates (Figure 1(**C**)). Their relative arrangements in either case did not show appreciable effect on the orientation of molecules adsorbed on either charged or uncharged graphite surface (as detailed in following). The distortion can be verified by the energy difference of 1.21 kJ/mole. (See adsorption energy section.) The two plates are separated by 3.35 Å in agreement with the experiment.[57,58]

Simulations are performed at the temperature (323 K) found essential in fabrication of electrode (by both binder) for best electroanalytical performance. This temperature is higher than the melting temperature of *n*-$C_{20}H_{42}$ (310 K) and $[C_4mim]PF_6$ (280 K) binders. At equilibrium, the average temperature of the simulation system in *NVE* ensemble is 318 K with low fluctuation (StDev=6.1 K). Simulations at higher $T$ (=353 K) are led to the same structural conclusion between double-$C_{600}$ and ionic liquid. We report the simulations at 323 K only.

**IL on Charged Graphite Plates.** The number 22 ILs, based on the optimal mass ratio (30/70, IL/graphite)[21,24] are initially distributed

randomly over outer surfaces of a charged double-$C_{600}$. With this ratio, only a monolayer of ion pairs is formed, with typically surface coverage of 85% on one side and 40% on the other side.

Correlation function, $g(r)$, is employed here to study the locale adsorption profile of ion-pairs on graphite, which form a two-dimensional monolayer. Spreading profile, structural relation and interaction of IL atoms with graphite atoms at different locations (particularly at the center (C_1), next to center (C_106), and two positions on edge planes (C_512) and (C_556)) are studied. (see Figure 1). $g(r)$'s for $N_1$ and $N_3$ atoms of imidazolium ring with respect to graphite local atoms are shown in Figures 3(**A**,**B**). The narrow width and large height of the short-range peaks indicate that $N_1$ and $N_3$ interaction with graphite is strong and of low dynamics. This solid-like feature is notably seen throughout, especially between imidazolium ring atoms and graphite atoms at center and near to the center. Notably the fabricated carbon paste electrodes are practically solid-like materials.[13,21]

Distances of closest approach (DCA) for all IL atoms approaching the graphite atom at different locations are calculated from the first peak of $g(r)$'s (see Table 1). DCA is simply the hard sphere diameter, and allows accessing precise local adsorption structure of IL binder on graphite surface. Most DCA values ($N_1$, 3.95 Å; $N_3$, 3.65 Å) are about graphene-graphene separation distance (3.35 Å). See Table 1.

C_1 atom is located symmetrically equidistance from all other graphite atoms, whereas several atoms equivalent to C_106 exist that their locus points form a circle centered at C_1 (Figure 1). Likewise, there are several carbon atoms equivalent to each labeled edge plane atoms. Hence, adsorption tendency of one location may differ from another because of two basic factors. First, each graphite C atom experiences characteristics local interatomic force, according to which the local adsorption energy is determined.

However, since simulation is performed under force field (including atomic charges) applied globally to all atoms, local interatomic force is not the basic factor for the preferential adsorption at one location. Second, the possibility of coordination of an anion $PF_6^-$ at certain location with maximum possible counter cation $[C_4mim]^+$ occurring naturally in the first shell, the second shell, etc., would determine the adsorption preferences at that location. Therefore, as time evolves, a $PF_6^-$ anion adsorbed dynamically on C_1 is coordinated by $[C_4mim]^+$ to achieve most stable configuration. Since all $PF_6^-$ anions compete for adsorption preferentially at the center, the probability of interaction with the center atom, especially the short-range interaction, is divided between all competing anions. These speculations are manifested as it can be seen that the first peak of the pair correlation function between every IL atom and C_1 (see also other figures) have either shorter amplitude or appear as a shoulder with short amplitude.

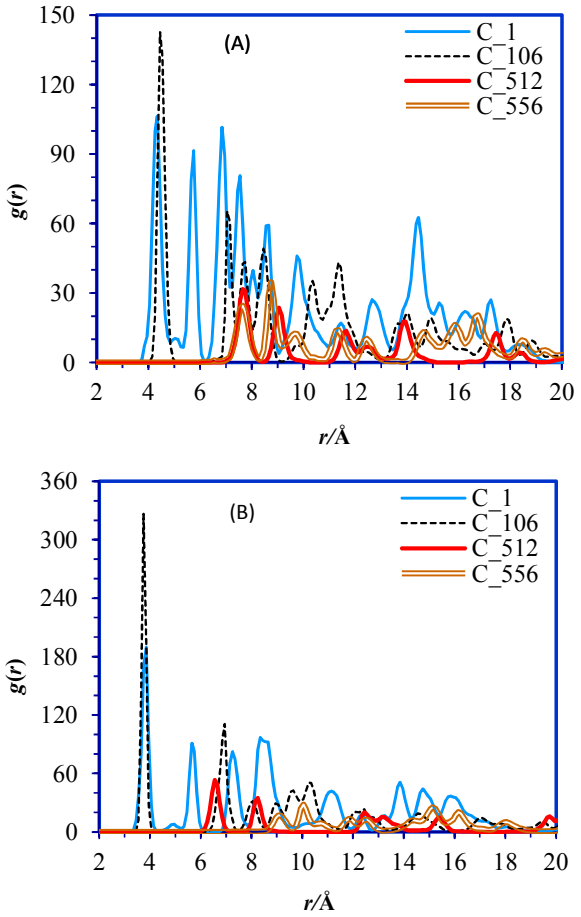


**Figure 3.** Simulated $g(r)$ between, (**A**) $N_1$ and, (**B**) $N_3$ and charged graphite atoms at different location. $T$=323 K.

**Table 1**. Simulated distances of closest approach (Å).

| IL atoms | graphite atoms | | | |
|---|---|---|---|---|
| | C_1 | C_106 | C_512 | C_556 |
| $N_1$ | 3.95 | 4.25 | 7.25 | 7.15 |
| $C_2$ | 3.55 | 4.25 | 7.35 | 7.65 |
| $N_3$ | 3.65 | 3.65 | 6.35 | 8.65 |
| $C_4$ | 3.25 | 3.25 | 5.65 | 8.45 |
| $C_5$ | 3.55 | 3.75 | 6.25 | 7.75 |
| $C_6$ | 3.45 | 3.85 | 6.35 | 9.65 |
| $C_7$ | 4.95 | 5.35 | 8.55 | 6.45 |
| $C_{10}$ | 5.75 | 7.85 | 7.65 | 5.85 |
| P | 4.35 | 5.85 | 8.55 | 7.45 |
| F | 3.25 | 4.35 | 6.85 | 6.15 |

On the other hand, interaction of $N_1$ and $N_3$ with C_106 at short-ranges is well structured with high probabilities. This can be attributed to the existence of several equivalent C_106 atoms.

The correlation of other imidazolium ring atoms $C_2$, $C_4$ and $C_5$ with C_1 are shown in Figures S1 to S3, respectively. For these cases, the correlations at short-range are rather low, though are



 

sizable with some dynamics at the mid-range. $C_4$ interaction is well structured with lower dynamics and higher probability than those of $C_2$ and $C_5$. Correlations of these atoms with C_106 at short-range is strong and well structured; of $C_4$ is the strongest. Overall, short-range interaction of all imidazolium ring atoms with C_106 is higher than with C_1. Presence of methyl and butyl group strictly hinders $C_2\cdots$C_1 interaction, as indicated by a lower correlation in Figure S1. On the other hand, the higher correlation of $C_4\cdots$C_1 and $C_5\cdots$C_1 may account for the lower correlation with the methyl group, e.g., $C_6\cdots$C_1 (Figure S4).

The alkyl group generally plays important role on physico-chemical properties of ILs and hence can provide valuable information. The $g(r)$ for $C_7$ (first $CH_2$) and $C_{10}$ (terminal $CH_3$) of the butyl group are shown in Figures S5 and S6. $C_{10}\cdots$C_1 is somehow featureless at all ranges and shows much weaker correlation than $C_7\cdots$C_1. Hence, alkyl group is likely directed away from center of plate. Furthermore, its interaction with different graphite surface regions is weaker than imidazolium ring.

Knowing that $[C_4mim]^+$ and $PF_6^-$ are tightly bonded ion-pair and that $[C_4mim]PF_6$ is highly hydrophobic,[33,59] the structural relation of anion atoms with respect to graphite surface is verified by pair correlation functions. P$\cdots$C_1 correlation is well structured, with high probability and low dynamics, at all ranges (Figure S7). Holding certain correlations between anion and the central (C_1 and C_106) atoms reflect anion-cation coordination capabilities. Earlier, *ab initio* quantum chemical calculations,[33] have demonstrated the simultaneous interaction of the anion $PF_6^-$ with the cation imidazolium ring and with the graphite surface.

F$\cdots$C_1 correlation is strong and conforms to P$\cdots$C_1 correlation. The triple peak at short range suggests interaction of three F atoms with surface (Figure S8). First peak position of P$\cdots$C_1 (4.45 Å) and of F$\cdots$C_1 (3.55 Å) indicates that anion approaches quit close to graphite surface. Considering DCA's (F$\cdots$C_1, 3.25 Å; F$\cdots$C_106, 4.35 Å, Table 1), it can be concluded that, consistent with earlier quantum chemical studies,[33] the $PF_6^-$ anion interacts with the imidazolium ring plane while tending to relax on the graphite surface. This simultaneous interaction requires tilting imidazolium ring with respect to graphite plane normal and is estimated to be by about 9.30° based on DCA's of ring atoms (Figure S9).

**Coordination Features.** Short-range peak values of $g(r)$'s are generally large, and demonstrate strong solid-like interaction of IL atoms with graphite surface. Considering also those long-range peaks for $N_1$, $N_3$, $C_2$, and $C_6$ atoms are spaced quite evenly leads to a coordinated type interaction with respect to the graphite central atoms. This coordination is indeed originated from the nature of cation-anion coordination interaction while interacting with the graphite surface. In the present case, adsorbed ion-pairs tend to interact with graphite central atoms, permitting to form a two-dimensional dense state comprising coordinated ion-pair rather than an expanded state with cations and anions spread all over the surface randomly. This property, inherent in most ILs, is responsible for ordered distribution of ion pairs forming monolayer on graphite surface. The feature is unique to the present case under study and does not necessarily extend as such in case of double or multi-layers adsorption. With a double layer, the second layer is derived into diffused configuration of anion and cation contrary to the orderly adsorbed first layer.[30] Therefore, these inherent coordination properties of IL plays essential role in the *monolayer adsorption structure* and the extent of interaction based on experimental condition.

**Correlation with the Edge Plane Atoms.** The extent of interaction and positioning of IL with respect to edge plane atoms are at the center of attention. Generally weak and featureless correlations with these atoms (typically C_512 and C_556) are seen at all ranges (Figures 3, S1 to S8). Even though the alkyl tail atom ($C_{10}$), which has weaker correlation with graphite center than other IL atoms, shows a very weak correlation with edge plans and avoids approaching edge planes. Therefore, ILs molecules tend to distribute densely over the middle of graphite surface in the form of a monolayer of the coordinated ion-pairs. The snapshot shown in Figure 4(**A**) indicates that the anion at the center is enwrapped by cations (within small circle), and in turn are enwrapped by anions (large circle). Therefore, under the experimental condition, such high coordination ability implies IL ion-pairs avoid approaching edge planes as much as possible. The present unique result is in excellent agreement and shed light, at atomic level, on the Figueiredo-Filho et al. experimental observation that claims a low coverage of edge plane sites at graphitic materials. Consequently, improved electrochemical properties and performance observed is due to an increment in the available edge plane. However, the value of edge coverage can be attributed to the geometry of graphite as also emphasized by these researchers.[60,61] The state of highly coordinated ion pairs obviously belongs to a highly stable state consistent with maximum possible long range electrostatic interaction between ions. This ordered distribution can be characterized geometrically by global and local coordination of the anion-cation as demonstrated by circles and pentagon in Figure 4. Characterization also involves the calculation of spatial distribution functions (SDFs) using 2500 collected configurational data. Each trajectory for SDF calculation is evaluated using the TRAVIS,[62] (with isosurface density of 0.5Å$^{-3}$), to further demonstrate coordination scheme by the map obtained as in Figures 4(**C**,**D**).

**IL Intercalated between Graphite Charged Plates.** Simulations are also performed for IL ion-pairs intercalated into the double-$C_{600}$ plates. With the same mass ratio (30/70, IL/graphite), a uniform bilayer of ILs confined between the two plates is formed. Under such circumstance, the simulation results (structure and dynamics of intercalated IL binder) take the advantage of more data available for analysis. Noteworthy, electric field of both plates influence norm of structure and dynamics of intercalated species. In spite of these, results of this part (followings) are consistent with the previous part.

In general, the $g(r)$'s (Figures S10-S19) look more like systems normally encountered in simulations of bulk matter comprising large number of molecules. Moreover, results are similar to the previous case, except that the peaks are broader, their values at long-range are slightly higher and their positions shifted to higher distances. For instance, compared to previous case, the peak at long-range for $N_1\cdots$C_1 (Figure S10) is now shifted (by 2 Å) to higher distance. As a result, the interaction of all IL atoms with the edge plane carbon atoms increases a little bit more; their $g(r)$'s indicate a rather well-structured configuration at short range. A discussion in terms of adsorption energy will follow.

The anion is highly correlated with C_1 at short-ranges with characteristics coordination at mid- and long-range. However, P$\cdots$C_1 and P$\cdots$C_106 correlations are diminished to some extent at long-range (Figure S18). In the same way, P$\cdots$C_512 and P$\cdots$C_556 correlations are featureless at short-ranges, indicating

that the anion seriously avoids approaching the edge planes. A snapshot of the equilibrated ensemble is shown in Figure 5(**A**). DCA's values (Table S3) and the cation-anion represented by spatial distribution function (Figure 5(**B**)) all support that the intercalated IL atoms avoid adsorbing on edge planes. With the ILs intercalated, the plates are slightly distorted with respect to each other (Figure 5(**A**)), contrary to the case with IL over the plates, leading to liquid-like dynamics of the intercalation. This can account in part for the slight increase in the IL correlation with the edge plane carbon atoms. The average separation of the two plates is estimated to be almost 10 Å.

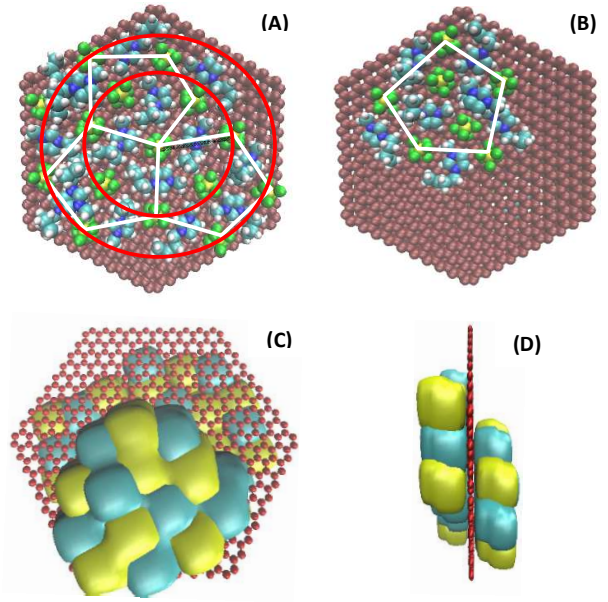


**Figure 4.** Snapshot of ensemble of IL adsorbed over double-$C_{600}$ charged graphite at equilibrium. (**A**) and (**B**): Top view of both sides. Global (circle) and local (pentagon) coordinations are evident. Similar distribution is held with uncharged plates. Online color: graphite C, brown; IL C, cyan; H, white; N, dark blue; F, green; P, yellow. (**C**) and (**D**): SDF map of $[C_4mim]^+$ cation (cyan) and $PF_6^-$ anion (yellow). Top view of both $C_{600}$ plates can be seen in (**C**); side view in (**D**) shows the relative structure of edge plane atoms left uncovered. Only one $C_{600}$ plate is shown for clarity.

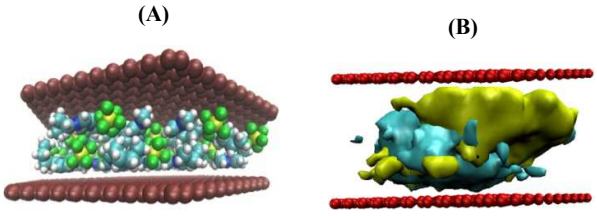


**Figure 5.** (**A**) Snapshot of IL between double-$C_{600}$ charged graphite plates. Online color: graphite C, brown; IL C, cyan; H, white; N, dark blue; F, green; P, yellow. (**B**) Representation of spatial distribution function of $[C_4mim]^+$ cation (cyan) and $PF_6^-$ anion (yellow).

**Paraffine on Charged Graphite Plates.** To illuminate the better performance of carbon paste electrode involving IL, similar simulations are performed using *n*-$C_{20}H_{42}$ as the conventional paraffinic binder. The ensemble constructed containing 22 paraffine molecules per a double-$C_{600}$ also corresponds to the practically optimized mass ratio (30/70, paraffine/graphite).[21,24] The study is based on analyzing relative structure and dynamics of different paraffine carbon atoms: two identical terminal atoms ($C_{P1}$), two identical $C_5$ and $C_{15}$ ($C_{P5}$) and the middle atom ($C_{P10}$) (labels shown in Figure 2). Since the paraffine is not well-defined suitably for statistical mechanical analysis as in the case of IL, therefore, the interaction with the substrate graphite cannot be defined uniquely and the analysis is also lend a hand by visual inspection of equilibrated simulation ensemble.

Compared with IL, correlation of paraffine atoms with graphite at different locations are substantially of lower probability and higher dynamics (Figures 6(**A**), (**B**)). Additionally, there exist comparable structured short-range correlations between paraffine and graphite atoms at the edge planes as well as at the center. For instance, $C_{P1}\cdots C\_1$ correlation at the short range is to a good deal comparable with those of $C_{P1}\cdots C\_512$ and $C_{P1}\cdots C\_556$ (Figure 6(**A**)). Also, the position of all peaks at short-range is nearly the same. The $g(r)$ for $C_{P10}$ (Figure 6(**B**)) also confirms distribution of paraffine over all locations evenly. Short-range peaks are all quite similar with comparable probabilities, though probabilities for $C_{P10}\cdots C\_512$ and $C_{P10}\cdots C\_556$ are smaller than for $C_{P1}$, which can be attributed to the difference in the relative locations of $C_{P10}$ and $C_{P1}$.

Nontheless, peaks are not quite similar because, a paraffine chain can interacts effectively along a row of atoms shaped by honeycomb structure, and therefore, the chain can interact effectively along limited number of (three different but equivalent) directions over the substrate graphite (Figure 6(**C**)). Therefore, correlation of a given paraffine atom with edge plane carbon at different edges is not necessarily the same. Interestingly, $g(r)$'s at short ranges are the same and the DCAs (Table 2) of $C_{P1}$ with atoms at different graphite surface location are very close to one another. Therefore, paraffine molecules are distributed and adsorbed almost evenly over the center, sides, and the edge planes, as can be seen from two views of the conformation and orientation (Figures 7(**A**), (**B**)) and the SDF (Figure 7(**C**)). In some instances, the adsorbed paraffine chains tend to cover completely and or cut through the edge planes.

**Table 2.** The distance of closest approach (**Å**) of *n*-$C_{20}H_{42}$ atoms at different locations on graphite charged plates.

| paraffine atoms | graphite atoms | | | |
|---|---|---|---|---|
| | C_1 | C_106 | C_512 | C_556 |
| $C_{P1}$ | 3.35 | 3.45 | 3.45 | 3.25 |
| $C_{P10}$ | 3.55 | 3.55 | 3.55 | 3.65 |

**Paraffine intercalated between charged graphite plates.** In general, the results are similar to the case of paraffine molecules adsorbed on the surface of double-$C_{600}$ charged graphite plate, except for higher adsorption probability on edge plane atoms (S20 and S21). When confined between two plates, paraffine molecules are squeezed and pushed towards edge planes. Molecules are completely adsorbed over the inner surfaces, and cover center, sides and edge planes. The DCAs (Table S4) confirm a uniform adsorption. However, three honeycomb directions (Figure 6(**C**)) would pattern the spreading and effective interaction. The

correlation at long-ranges for $C_{P1}$···C_512 and $C_{P1}$···C_556 is high but not well-defined.

**Simulations Involving Uncharged Plates.** The resulted outlook is generalized by performing similar simulations involving uncharged graphite plates. A summary of the results indicates the IL in general shows the similar with slightly different adsorption properties: **1**) the corresponding $g(r)$ are less structured with lower peak values, representing slightly higher dynamics, **2**) alkyl atoms (except terminal atom) show a weaker correlation with the edge plane's atoms, **3**) imidazolium ring atoms have a more strong interaction with center and middle (C_1 and C_106) atoms. Overall, a strong correlation exists between atoms of IL and C_1 and C_106. The DCA values indicate ring atoms spread slightly more at longer distances. (IL on: Figures S22-S31; DCA, Table S5) (IL intercalated: Figures S32-S41; DCA, Table S6). Paraffine simulation outlook is very much similar with simulation involving charged graphite. (paraffine on: Figures S42, S43; DCA's, Table S7) (paraffine intercalated: Figures S44 and S45; DCA, Table S8)

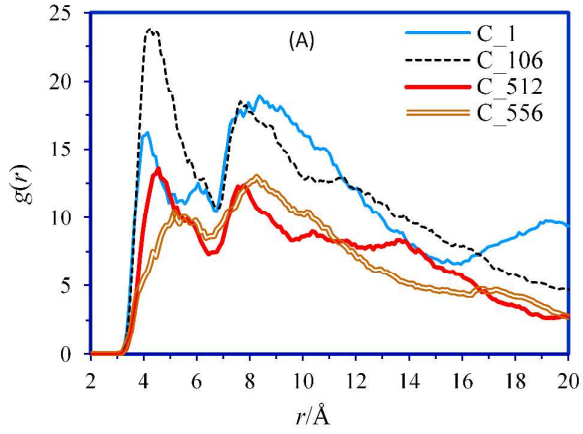


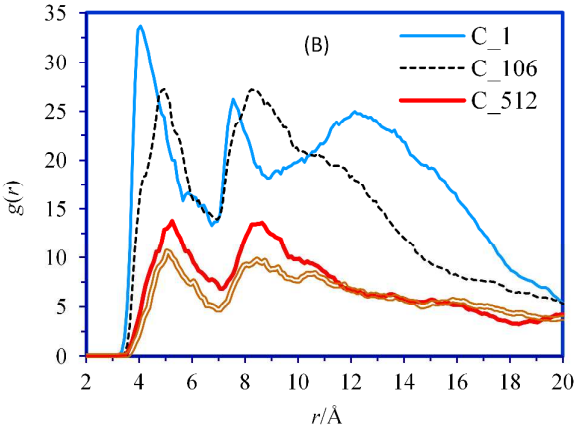


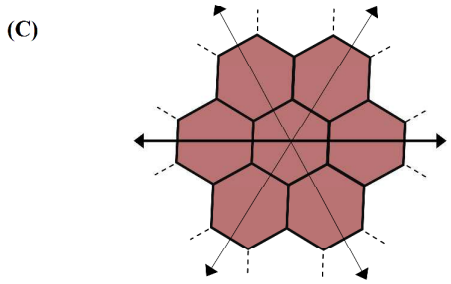


**Figure 6.** Simulated $g(r)$ between, (**A**) $C_{P1}$ and (**B**) $C_{P10}$ paraffine atom and double-$C_{600}$ charged graphite atoms at different location at 323 K; (**C**) Representation of possible orientations for paraffine adsorption on graphite.

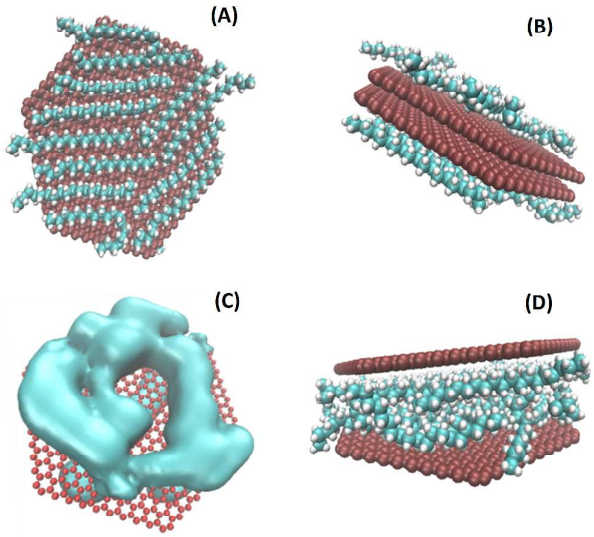


**Figure 7.** (**A**) and (**B**): Two views of the conformation and orientation of paraffine on double-$C_{600}$ charged graphite plates. (**C**) SDF map of paraffine on double-$C_{600}$ (only one plate is shown for clarity). (**D**) Side view of paraffine intercalated between charged plates.

**Adsorption Energies.** Energetics of the adsorption process conveys appreciable information suitable for comparative characterization of the binders quantitatively. The intermolecular interaction energy per mole ($E$) of binder-graphite is defined as the sum of molar van der Waals and Coulombic energies:

$$E = E_{vdW} + E_{Coul} \quad (5)$$

Then the adsorption energy ($E_{ads}$) can be calculated as the difference between energy of the whole system ($E$) and sum of energies of pure binder ($E_{Binder}$) and graphite ($E_{graphite}$):

$$E_{ads} = E - (E_{Binder} + E_{graphite}) \quad (6)$$

Calculated $E_{ads}$ for all eight simulations, shown in Table 3, indicates that simulated carbon past with IL binder is much more stable than with paraffine binder. For instance, IL binder placed on the charged graphite plates is more stable by about 846.55 kJ $mol^{-1}$ than paraffine binder. Furthermore, **1**) there is no appreciable difference in the energy of charged and uncharged cases when IL is

concerned, **2**) the intercalation (of the IL) contributes more to the stabilization by about 186.95 kJ mol$^{-1}$. The last two rows in Table 3 indicate the doubl-$C_{600}$ charged plates is more stable by 1.21 kJ/mole than the uncharged ones.

**Multilayer Adsorption of IL and Paraffine Binders.** The issue that may rise is how the practical occurrence of double layer and overwhelming multilayer adsorption under the fabrication condition may influence the conclusions already drawn. Hence, two more simulations are performed to explore the distribution and structural differences between monolayer and multilayer adsorption of each binder on the graphite surface. Keeping track of long-range coordination persisted in the two-dimensional solid-like state of adsorbed monolayer of IL, the outlook of short-range properties persisted in liquid-like state can be evaluated.

**Table 3.** Adsorption Energies.

| binder | graphite substrate | | $E_{inter}$ /kJ mol$^{-1}$ |
|---|---|---|---|
| | charged | uncharged | |
| $[C_4mim]PF_6$ | over | | -1414.16 |
| $[C_4mim]PF_6$ | intercalated | | -1601.11 |
| $[C_4mim]PF_6$ | | over | -1412.65 |
| $[C_4mim]PF_6$ | | intercalated | -1689.27 |
| *n*-$C_{20}H_{42}$ | over | | -567.61 |
| *n*-$C_{20}H_{42}$ | intercalated | | -104.42 |
| *n*-$C_{20}H_{42}$ | | over | -580.86 |
| *n*-$C_{20}H_{42}$ | | intercalated | -375.28 |
| - | double-$C_{600}$ | | -638.78 |
| - | | double-$C_{600}$ | -637.57 |

The equilibrated ensemble of a double-$C_{600}$ charged graphite, initially immersed in a three dimensional matrix of 216 binder molecules, is shown in Figure 7(**A**) and (**B**) for IL and paraffine binders, respectively. The binder is quantitatively good enough to form a multilayer. It is seen that even in the case of multilayer adsorption, where coordination properties are not well extend to long-range due to screening, yet ILs binder avoid extensive approach and covering the graphite edge planes. On the contrary, paraffine multilayer adsorption extends arbitrary over graphite surface and the edge planes. However, three points should be considered before trying any conclusion. First, both binders are hydrophobic, but of different nature. IL tends to spread leading to a drop formation (of high contact angle) but paraffine spread tending to swell the graphite (with low contact angle). Second, the IL is much denser than paraffine (1.378,[63] versus 0.860 g/cm$^3$,[64] at 298K). Third, correlation function in IL case produces independent results characteristics of a system with highly coordinated first layer and weakly coordinated subsequent layer.

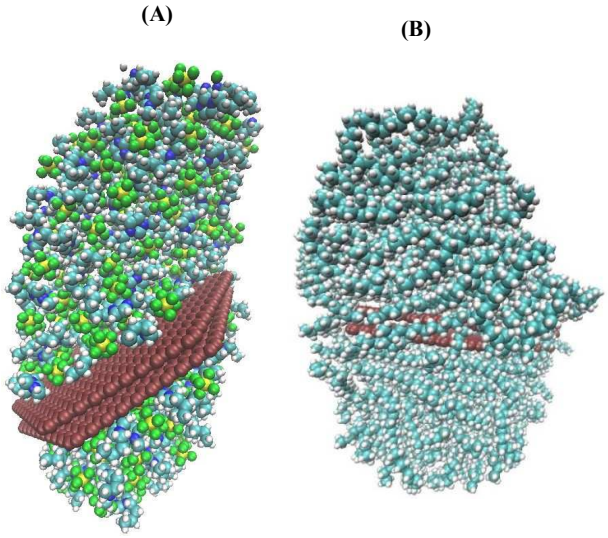


Figure 8. Equilibrated ensemble of double-$C_{600}$ charged plates immersed in, (A) IL and, (B) in paraffine**.**

Drop formation may naively be thought as a result of hydrophobicity of IL on hydrophob graphite, but this does not justify adequately hydrophob-paraffine drop formation of different nature.

## Conclusions

A direct quantitative and qualitative comparison of IL properties with those of an organic liquid counterpart as binders in carbon paste electrode, made here by MD simulation for the first time, produces rewarding results.

Either ionic liquid or paraffine binder molecules are immobilized on graphite surface when fabricated as carbon paste electrode. In IL case, this immobilization is, however, contributed by a coordination capability (contrary to paraffine) that drives cation-anion into a 2-D solid-like matrix and the long-range Coulombic interaction pull them together to allow the highest possible long range coordination. Strong coordination occurs under the condition that translational degrees of freedom are reduced and restricted to two-dimensional surface.

The simulation based on experimental mass ratio found practically for best electroanalytical performance corresponds to only monolayer formation by both type binder, confirming improved electrochemical properties for the IL binder. However, edge planes aren't approached and are left uncovered by the IL binder, while covered by the paraffine binder. Multilayer adsorption of both binders also demonstrates the same approaching to the edge plane, which confirms the phenomena as inherent and not deterioration by the change in the condition. Considering that the electrons move through (C=C) $\pi-$ system of graphite plate, the results of this work shed light on the observed enhancement of the electrochemical performance, attributing to the edge plane carbon atom left uncovered (ready for electron transfer) when IL is used as binder. This is in line with the literature on graphene which indicates that the edge of graphene is particularly more reactive than basal plane (due to the greater electron density) and the



 

amount of edge planes dictate the overall electrochemical properties.[65,66]

The relative microstructure of the edges (with the IL binder) used to account for the enhanced electrochemical property relies on the coordination properties simulated. This is consistence with the new experimental finding of graphite exfoliation by IL, which believed to occur during fabrication process and argued to leave graphene with sharp knife-edge structure of nanometer-sized-thick identified by SEM and TEM.[25] A conjecture here is that monolayer formation by the virtue of coordination property of the IL prevents coalescence of graphene sheet,[60] (to merge as graphite) when is used in fabrication of carbon paste electrode.

By the coordination properties enhanced strongly in monolayer formation, the IL can easily offer a molecular-level built-in technology suitable for ease of high electron transfer in electroanalytical devices.

## Acknowledgements

The authors are indebted to the research council of the Shiraz University for financial support. Cluster computing facilities are granted in part by Enhanced Oil Recovery (EOR) Center of the College of Engineering. Helps on the subject matter from analytical chemistry lab are gratefully acknowledged.

## Notes and references

1. T. Welton, *Chem. Rev.* 1999, **99**, 2071.
2. R.D. Rogers, K.R. Seddon, *ACS Symposium Series*. 2002, **818**, 474.
3. P. Wasserscheid, T. Welton, *Wiley-VCH*, 2003.
4. F. Endres, *Chem. Phys. Chem.*, 2002, **3**, 144.
5. M.C. Buzzeo, R.G. Evans, R.G. Compton, *Chem. Phys. Chem.,* 2004, **5**, 1106.
6. F. Zhao, X. Wu, M. Wang, Y. Liu, L. Gao, S. Dong, *Anal. Chem.* 2004, **76**, 4960.
7. J. Liu, F. Wang, L. Zhang, X. Fang, Z. Zhang, *Renewable Energy* 2014, **63**, 519.
8. D.L. Astolfi, F.C. Mayville, *Tetrahedron Lett*., 2003, **44**, 9223.
9. Z. Yang, W. Pan, *Enzyme Microb Tech.*, 2005, **37**, 19.
10. Y. Liu, L. Shi, M. Wang, Z. Li, H. Liu, J. Li, *Green Chem.*, 2005, **7**, 655.
11. O. Schneider, A. Bund, A. Ispas, N. Borissenko, S. Z.E. Abedin, F. Endres, *J. Phys. Chem. B.*, 2005, **109**, 7159.
12. E. Roznіecka, G. Shul, J. Sirieix-Plenet, L. Gaillon, M. Opallo, *Electrochem. Commun.*, 2005, **7**, 299.
13. Y. Zhao, Y. Gao, D. Zhan, H. Liu, Q. Zhao, Y. Kou, Y. Shao, M. Li, Q. Zhuang, Z. Zhu, *Talanta*, 2005, **66**, 51.
14. H. Liu, P. He, Z. Li, C. Sun, L. Shi, Y. Liu, G. Zhu, J. Li, *Electrochem. Commun.*, 2005, **7**, 1357.
15. C. Lagrost, L. Preda, E. Volanschi, P.H. Hapiot. *J. Electroanal., Chem.*, 2005, **585**, 1.
16. R.T. Kachoosangi, M.M. Musameh, I. Abu-Yousef, J.M. Yousef, S.M. Kanan, L. Xiao, S.G. Davies, A. Russell, R.G. Compton, *Anal. Chem.*, 2009, **81**, 435.
17. R.T. Kachoosangi, G.G. Wildgoose, R.G. Compton, *Electroanalysis.*, 2007, **19**, 1483.
18. R.T. McCreery, A.J. Bard, eds. *Electroanalytical Chemistry*, 1st ed, Dekker, New York. 1991, **17**, 221.
19. R.L. McCreery, P.T. Kissinger, W.R. Heineman, eds. *Laboratory Techniques in Electroanalytical Chemistry*, 2nd ed, Dekker, New York, 1996, Chapter 10.
20. J. Wang, *Electroanalytical Chemistry*, 2nd ed, Wiley, New York, 2000.
21. N. Maleki, A. Safavi, F. Tajabadi, *Anal. Chem.*, 2006, **78**, 3820.
22. H. Goto, E. Uesugi, R. Eguchi, A. Fujiwara, Y. Kubozono, *Nano Lett.* 2013, **13**, 1126.
23. C.E. Banks, R.G. Compton, *Analyst*, 2005, **130**, 1232.
24. M. Musameh, J. Wang, *Analytica Chimica Acta*, 2008, **606**, 45.
25. X. Zhang, M. Li, Y. Cui, J. Zhu, J. Zhao, B. Chen, K. Qu. *Int. J. Electrochem. Sci.*, 2013, **8**, 4839.
26. S. Maolin, Z. Fuchun, W. Guozhong, F. Haiping, W. Chunlei, C. Shimou, Z. Yi, H. Jun, *J. Chem. Phys.*, 2008, **128**, 134504.
27. S.A. Kislenko, I.S. Samoylov, R.H. Amirov, *Phys. Chem. Chem. Phys.*, 2009, **11**, 5584.
28. M. Sha, G. Wu, H. Fang, G. Zhu, Y. Liu, *J. Phys. Chem. C*, 2008, **112**, 18584.
29. M. Sha, G. Wu, Y. Liu, Z. Tang, H. Fang, *J. Phys. Chem. C.*, 2009, **113**, 4618.
30. M.H. Fedorov, R.M. Lynden-Bell, *Phys. Chem. Chem. Phys.,* 2012, **14**, 2552.
31. Z. Hu, J. Vatamanu, O. Borodinb, D. Bedrova, *Phys. Chem. Chem. Phys.*, 2013, **15**, 14234.
32. R. Burt, G. Birkett, X.S. Zhao, *Phys. Chem. Chem. Phys.,* 2014, **16**, 6519.
33. M.H. Ghatee, F. Moosavi, *J. Phys. Chem. C*, 2011, **115**, 5626.
34. Y. Zhao, Z. Hu, *J. Phys. Chem. B.*, 2013, **117**, 10540.
35. A.S. Pensado, F. Malberg, M.F. Costa Gomes, A.A.H. Padua, J. Fernandez, B. Kirchner, *RSC Adv.*, 2014, **4**, 18017.
36. A.L. Pak, E. Paek, G.S. Hwang, *J. Phys. Chem. C,* 2014, **118**, 21770.
37. E. Paek, A.J. Pak, G.S. Hwang, *J. Electrochem. Soc*. 2013, **160**, A1.
38. B.C. Wood, T. Ogitsu, M. Otani, J. Biener, *J. Phys. Chem. C* 2014, **118**, 4.
39. E. Paek, A.J. Pak, K.E. Kweon, G.S. Hwang, *J. Phys. Chem. C*, **2013**, *117*, 5610−5616.
40. D.A.C. Brownson, L.J. Munro, D.K. Kampouris, C.E. Banks, *RSC Adv*. 2011, **1**, 978.

41. W. Song, X. Ji, W. Deng, Q. Chen, C. Shen, C.E. Banks, *Phys. Chem. Chem. Phys*., 2013, **15**, 4799–4803.

42. S. Banerjee, J. Shim, J. Rivera, X. Jin, D. Estrada, V. Solovyeva, X. You, J. Pak, E. Pop, N. Aluru, *ACS Nano* 2013, **7**, 834.

43. J. Vatamanu, L. Cao, O. Borodin, *J. Phys. Chem. Lett*., 2011, **2**, 2267.

44. L. Xing, J. Vatamanu, G.D. Smith, D. Bedrov, *J. Phys. Chem. Lett*., 2012, ***3***, 1124.

45. X. Jia, J. Campos-Delgado, M. Terrones, V. Meunier, M.S. Dresselhaus, *Nanoscale* 2011, **3**, 86.

46. F. Dietz, N. Tyutyulkov, G. Madjarova, K. Müllen, *J. Phys. Chem.* B, 2000, **104**, 1746.

47. A. Staykova, L. Gehrgelb, F. Dietza, N.Z. Tyutyulkova, *Naturforsch*., 2003, **58**, 965.

48. S. Alavi, D. Thompson, *J. Chem. Phys.* 2005, **122**, 154704.

49. M.J. Frisch, G.W. Trucks, H.B. Schlegel, et al. GAUSSIAN 03, Revision C. 02. GAUSSIAN Inc., Wallingford, CT. 2004.

50. J.N. Canongia Lopes, J. Deschamps, A.A.H. Pádua, *J. Phys. Chem. B*, 2004, **108**, 2038.

51. L. William, W.L. Jorgensen D.S. Maxwell, J. Tirado-Rives, *J. Am. Chem. Soc.*, 1996, **118**, 11225.

52. W.D. Cornell, P. Cieplak, C.I. Bayly, I.R. Gould, K.M. Merz, D.M. Ferguson, D.C. Spellmeyer, T. Fox, J.W. Caldwell, P.A. Kollman, *J. Am. Chem. Soc.* **1995**, **117**, 5179.

53. W. Smith, T.R. Forester, I.T. Todorov, M. Leslie, *J. Molec. Graphics*., 1996, **14**, 136.

54. K.R. Ratinac, W. Yang, J. Gooding, J. *Electroanalysis.*, 2011, **23**, 803.

55. M. Tunckol, J. Durand, P. Serp, *Carbon*, 2012, **50**, 4303.

56. D.W. Kimmel, G. LeBlanc, M.F. Meschievitz, D.E. Cliffel, *Anal. Chem.*, 2012, **84**, 685.

57. K. Kinoshita, *Carbon Electrochemical and Physiochemical Properties*, Wiley, 1988.

58. F. Rozploch, J. Patyk, J. Stankowski, *Acta Physica Polonica A,* 2007, **112**, 557.

59. M.H. Ghatee, A.R. Zolghadr, *J. Phys. Chem. C*, 2013, **117**, 2066.

60. L.C.S. Figueiredo-Filho, D.A.C. Brownson, M. G´omez-Mingot, J. Iniesta, O. Fatibello-Filho, C. E. Banks, *Analyst*, 2013, **138**, 6354.

61. L.C.S. Figueiredo-Filho, D.A.C. Brownson, O. Fatibello-Filho, C.E. Banks, *Analyst*, 2013, **138**, 4436.

62. M. Brehm, B. Kirchner, *J. Chem. Inf. Model.*, 2011, **51**, 2007.

63. M.H. Ghatee F. Moosavi, A.R. Zolghadr, R. Jahromi, *Ind. Eng. Chem. Res.*, 2010, **49**, 12696.

64. http://www.apar.com/PDFs/LIQUID%20PARAFFIN%20-%20IP_BP_EP.pdf (visited Dec. 13, 2014).

65. D.A.C. Brownson, D. K. Kampouris, C. E. Banks, *Chem. Soc. Rev.*, 2012, **41**, 6944.

66. P. M. Hallam, C. E. Banks, *Phys. Chem. Chem. Phys*., 2011, **13**, 1210.